Volume 1 | Number 1 | Jan 2013 | Pages 1–100

Journal of
Materials Chemistry A

Materials for energy and sustainability
www.rsc.org/materialsA

Li⁺

ROYAL SOCIETY
OF CHEMISTRY

ROYAL SOCIETY
OF CHEMISTRY

www.rsc.org/materialsA

Journal Name

ARTICLE

Improved oxide-ion conductivity of NdBaInO$_4$ by Sr doping

Kotaro Fujii,[a] Masahiro Shiraiwa,[a] Yuichi Esaki,[b] Masatomo Yashima,[a,*] Su Jae Kim,[c] Seongsu Lee[c]

Oxide-ion conductivity of NdBaInO$_4$ has been increased by Sr doping. Nd$_{0.9}$Sr$_{0.1}$BaInO$_{3.95}$ showed highest electrical conductivity among Nd$_{1-x}$Sr$_x$BaInO$_{4-x/2}$ (x = 0.0, 0.1, 0.2, or 0.3). The oxide-ion conductivity σ_{ion} of Nd$_{0.9}$Sr$_{0.1}$BaInO$_{3.95}$ (σ_{ion} = 7.7 × 10^{-4} S cm^{-1}) is about 20 times higher than that of NdBaInO$_4$ (σ_{ion} = 3.6 × 10^{-5} S cm^{-1}) at 858 °C, and the activation energy of oxide-ion conduction is a little lower for Nd$_{0.9}$Sr$_{0.1}$BaInO$_{3.95}$ (0.795(10) eV) than that for NdBaInO$_4$ (0.91(4) eV). The structural analysis based on neutron powder diffraction data revealed that the Sr exists at Nd site and oxygen vacancies were observed in Nd$_{0.9}$Sr$_{0.1}$BaInO$_{3.95}$. This result indicates that the increase of the oxide-ion conductivity is mainly due to the increase of the carrier concentration. The bond valence-based energy landscapes indicated two-dimensional oxide-ion diffusion in the (Nd,Sr)$_2$O$_3$ unit on the *bc*-plane and a decrease of the energy barrier by the substitution of Nd with Sr cations.

INTRODUCTION

Oxide-ion conductors, which include pure ionic conductors and mixed oxide-ion and electronic conductors, attract significant interest because of their varied uses in oxygen separation membranes and cathodes for solid-oxide fuel cells (SOFCs).[1] The oxide-ion conductivity is strongly dependent on the crystal structure and particularly the defects. At present, several structures, such as fluorites,[2,3] perovskites,[2,4] K$_2$NiF$_4$,[2,5] mellilites,[2,6] and apatites,[2,7] are known to show high oxide-ion conductivities. For further development of oxide-ion conductors is investigating materials with new types of structures. Recently, we have discovered a new structural family of oxide-ion conductor based on NdBaInO$_4$, a monoclinic *P*2$_1$/*c* perovskite-related phase with a layered structure.[8] In this study, we have successfully improved the oxide-ion conductivity of NdBaInO$_4$ by Sr doping at the Nd site, which aims to increase the concentration of oxygen vacancies (i.e., carriers for the oxide-ion conduction) and to lower the activation energy by exchanging Nd^{3+} with the larger Sr^{2+} cation. This study reports on the electrical conductivity and the crystal structure of Sr-doped NdBaInO$_4$. The electrical conductivity of NdBaInO$_4$ was also investigated again for comparison.

EXPERIMENTAL SECTION

Synthesis and characterization of the chemical composition.

Nd$_{1-x}$Sr$_x$BaInO$_{4-x/2}$ (x = 0.0, 0.1, 0.2, 0.3, and 0.4) compounds were synthesized by solid-state reactions. Nd$_2$O$_3$ (99.95% purity) and BaCO$_3$ (99.9% purity) from Kanto Chemical Co. Inc., SrCO$_3$ and In$_2$O$_3$ (both 99.9% purity) from Kojundo Chemical Lab. Co., Ltd. were accurately weighted in 1-*x* : 1 : *x* : 1 cation molar ratios, and they were ground using a planetary ball mill (Fritsch, P7) for 30 min. The mixtures were calcined for 8 h in air for decarbonization. Then, the calcined mixtures were milled again for 30 min and uniaxially pressed into pellets at about 50 MPa. These pellets were sintered in air at 1400 °C for 24 h.

The cation ratio of Nd$_{0.9}$Sr$_{0.1}$BaInO$_{3.95}$ was confirmed by inductively-coupled plasma optical emission spectrometry (ICP-OES) as Nd : Sr : Ba : In = 0.919(8) : 0.0996(9) : 0.992(3) : 0.989(9), which agreed with the average chemical composition of the starting mixture, Nd : Sr : Ba : In = 0.9 : 0.1 : 1 : 1 within 3σ. Here, the σ is the standard deviation of the measured chemical composition and the number in the parenthesis is the last digit of σ.

Thermogravimetric analyses (TGA) of NdBaInO$_4$ and Nd$_{0.9}$Sr$_{0.1}$BaInO$_{3.95}$ in Ar flow (50 mL min^{-1}) were conducted using a Bruker-AXS TG-DTA2020SA instrument with heating and cooling rates of 10 °C min^{-1}. The TG measurements were
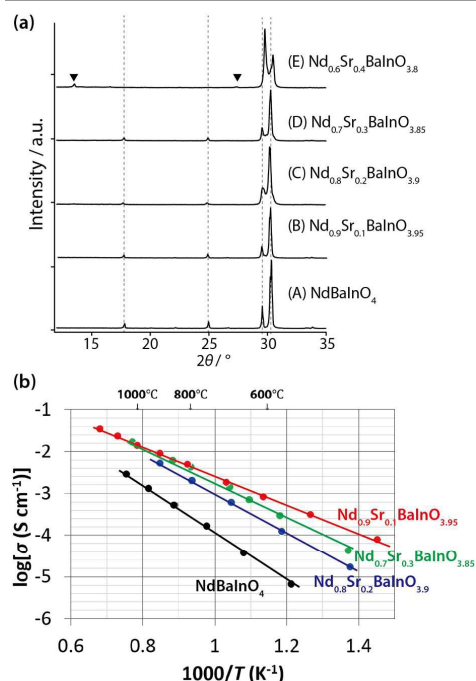
Figure 1. (a) X-ray powder diffraction patterns of (A) NdBaInO$_4$, (B) Nd$_{0.9}$Sr$_{0.1}$BaInO$_{3.95}$, (C) Nd$_{0.8}$Sr$_{0.2}$BaInO$_{3.9}$, (D) Nd$_{0.7}$Sr$_{0.3}$BaInO$_{3.85}$, and (E) Nd$_{0.6}$Sr$_{0.4}$BaInO$_{3.8}$. The dashed lines indicate the peak positions of the pure NdBaInO$_4$ phase. The black triangles show additional peaks that only appeared in Nd$_{0.6}$Sr$_{0.4}$BaInO$_4$. (b) Total electrical conductivities of NdBaInO$_4$ (black), Nd$_{0.9}$Sr$_{0.1}$BaInO$_{3.95}$ (red), Nd$_{0.8}$Sr$_{0.2}$BaInO$_{3.9}$ (blue), and Nd$_{0.7}$Sr$_{0.3}$BaInO$_{3.85}$ (green) measured in air.

repeated three times to confirm the reproducibility and minimize artefacts from adsorbed species such as water.

Electrical conductivity measurements.

The electrical conductivities of Nd$_{1-x}$Sr$_x$BaInO$_{4-x/2}$ (x = 0.0, 0.1, 0.2, and 0.3) were measured using a DC 4-probe method using sintered pellets (ca 4.4 mm $\phi \times$ 30 mm with densities in the range of 90%–95% of theoretical density) with Pt electrodes over the temperature range from 400 °C to 1200 °C in air. The oxygen partial pressure $P(O_2)$ dependence of the electrical conductivities of NdBaInO$_4$ and Nd$_{0.9}$Sr$_{0.1}$BaInO$_{3.95}$ were measured at 858 °C using N$_2$/H$_2$, N$_2$/CO$_2$, and N$_2$/O$_2$ gas mixtures. The $P(O_2)$ was monitored by an oxygen sensor that was set close to the sample. The oxide-ion conductivities of NdBaInO$_4$ and Nd$_{0.9}$Sr$_{0.1}$BaInO$_{3.95}$ were measured from 610 °C to 1100 °C under a $P(O_2)$ = 3.6±2.6 × 10^{-17} atm for NdBaInO$_4$ and $P(O_2)$ = 8.8±6.2 × 10^{-14} atm for Nd$_{0.9}$Sr$_{0.1}$BaInO$_{3.95}$.

Neutron and synchrotron X-ray diffraction measurements.
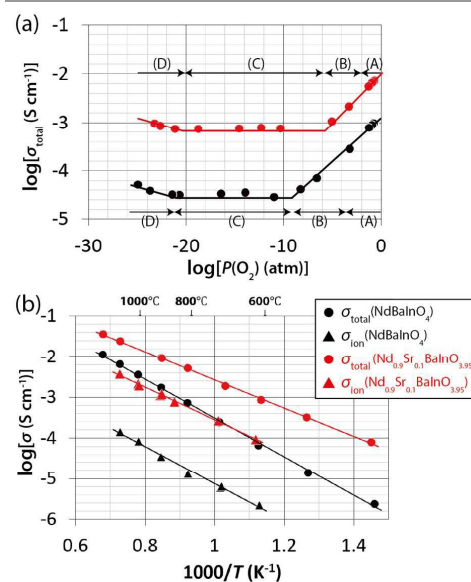
Figure 2. (a) Partial oxygen pressure $P(O_2)$ dependence of the total electrical conductivity σ_{total} (858 °C) of NdBaInO$_4$ (black) and Nd$_{0.9}$Sr$_{0.1}$BaInO$_{3.95}$ (red). The dominant carriers are electron holes in the $P(O_2)$ region [A], oxide ions and electron holes in [B], oxide ions in [C] and electrons in [D]. (b) Arrhenius plots of the total conductivity σ_{total} (circles) and ionic conductivity σ_{ion} (triangles) of NdBaInO$_4$ (black) and Nd$_{0.9}$Sr$_{0.1}$BaInO$_{3.95}$ (red). σ_{total} values were measured in air and σ_{ion} values were measured under $P(O_2)$ = 3.6±2.6 × 10^{-17} atm for NdBaInO$_4$ and $P(O_2)$ = 8.8±6.2 × 10^{-14} atm for Nd$_{0.9}$Sr$_{0.1}$BaInO$_{3.95}$.

Synchrotron X-ray powder diffraction (XRPD) measurements were conducted using a Debye–Scherrer camera with an imaging plate on beam line BL19B2 at SPring-8 (27 °C; wavelength = 0.399662(2) Å).[9] Room temperature time-of-flight (TOF) neutron powder diffraction (NPD) measurements (24 °C) were performed by the iMATERIA diffractometer of the J-PARC facility, Tokai, Japan.[10] High-temperature angle dispersive-type NPD measurements (800 °C using a vacuum furnace; wavelength = 1.83432(4) Å) were performed using the neutron powder diffractometer HRPD installed at HANARO reactor, KAERI, Korea.[11]

RESULTS AND DISCUSSION

XRPD patterns of Nd$_{1-x}$Sr$_x$BaInO$_{4-x/2}$ (x = 0.0, 0.1, 0.2, 0.3, and 0.4) identified the final products to be monoclinic $P2_1/c$ NdBaInO$_4$ phase, except x = 0.4, which showed a different XRPD pattern with additional peaks, indicating possible saturation of the dopant within the NdBaInO$_4$ structure (Figure 1a). We found that the total electrical conductivity of Nd$_{0.9}$Sr$_{0.1}$BaInO$_{3.95}$ is higher than that of NdBaInO$_4$, Nd$_{0.8}$Sr$_{0.2}$BaInO$_{3.9}$, and Nd$_{0.7}$Sr$_{0.3}$BaInO$_{3.85}$ (Figure 1b).

Comment [M1]: 図1を差し替える（欠けてる。酸素濃度が間違い3か所）

Journal Name

ARTICLE

Table 1. Crystallographic Data of $Nd_{0.9}Sr_{0.1}BaInO_{3.95}$.

Source and facility	TOF* Neutron iMATERIA, J-PARC	Synchrotron BL19B2, SPring-8	Neutron HRPD, HANARO	Ref. [7]
Chemical formula		$Nd_{0.9}Sr_{0.1}BaInO_{3.95}$	$Nd_{0.9}Sr_{0.1}BaInO_{3.90}$	$NdBaInO_{4.00}$
Formula weight		453.92		460.39
Temperature / ℃	24	27	800	20
Wavelength / Å	Time of Flight ($d = 0.494−5.223$ Å)	0.399662(2)	1.83432(4)	
Crystal system		Monoclinic		Monoclinic
Space group		$P2_1/c$		$P2_1/c$
a / Å	9.106468(17)	9.10285(12)	9.2060 (19)	9.09538(3)
b / Å	6.050490(11)	6.04769(5)	6.0999(11)	6.04934(2)
c / Å	8.268786(19)	8.26670(9)	8.2984(17)	8.25620(2)
β / °	103.40613(14)	103.3924(9)	103.057(12)	103.4041(3)
Unit-cell volume / Å^3	443.184(2)	442.716(8)	453.95 (15)	441.89(2)
Z		4		4
Calculated density / Mg m^{-3}	6.81	6.81	6.64	6.92
R_{wp}	0.0417	0.0230	0.0362	
R_p	0.0360	0.0150	0.0280	−
Goodness of Fit	1.838	1.000	1.860	−
R_B	0.0439	0.0139	0.0297	−
R_F	0.0213	0.0117	0.0156	−

* TOF: Time-of-Flight

Table 2. Atomic Coordinates and Atomic Displacement Parameters of $Nd_{0.9}Sr_{0.1}BaInO_{3.95}$ Obtained from the Time-Of-Flight Neutron Powder Diffraction Data (iMATERIA, J-PARC).

Site label X	atom Y	$g(Y, X)$ *	x	y	z	U (Å^2) **
Nd	Nd	0.9	0.45269(5)	0.74731(11)	0.10734(6)	0.00819 (U_{eq})***
	Sr	0.1				
Ba	Ba	1	0.14825(7)	0.25034(18)	0.0328(11)	0.00933 (U_{eq})
In	In	1	0.83211(9)	0.2545(2)	0.20649(14)	0.0030(19)
O1	O	0.9875	0.18155(8)	0.80285(9)	0.04782(12)	0.01422 (U_{eq})
O2	O	0.9875	0.98669(11)	0.98872(17)	0.26951(12)	0.00988 (U_{eq})
O3	O	0.9875	0.38341(9)	0.5429(13)	0.32909(11)	0.01730 (U_{eq})
O4	O	0.9875	0.65046(8)	0.50812(15)	0.12937(11)	0.01549 (U_{eq})

Site label X	U_{11} (Å^2)****	U_{22} (Å^2)	U_{33} (Å^2)	U_{12} (Å^2)	U_{13} (Å^2)	U_{23} (Å^2)
Nd	0.0065(3)	0.0051(2)	0.0063(3)	0.0001(3)	−0.0008(2)	0.0020(3)
Ba	0.0078(3)	0.0018(3)	0.0106(4)	0.0010(5)	0.0032(3)	0.0019(5)
O1	0.0170 (4)	0.0148(5)	0.0094(3)	0.0055(4)	0.0064(3)	0.0077(5)
O2	0.0048(3)	0.0090(3)	0.0148(5)	0.0056(3)	−0.0000(3)	0.0048(5)
O3	0.01516(5)	0.0194(5)	0.0131(5)	0.0059(4)	0.0016(4)	0.0032(5)
O4	0.0091(4)	0.0142(5)	0.0220(5)	0.0060(4)	−0.0041(4)	−0.007(4)

* $g(Y, X)$: Occupancy factor of atom Y at the X site. ** Atomic displacement parameter. *** Equivalent isotropic atomic displacement parameter. **** U_{ij}: Anisotropic atomic displacement parameter.

Therefore, we focused on the $Nd_{0.9}Sr_{0.1}BaInO_{3.95}$ composition for further detailed studies.

Figure 2a shows the $P(O_2)$ dependence of the total electrical conductivity σ_{total} of $NdBaInO_4$ and $Nd_{0.9}Sr_{0.1}BaInO_{3.95}$ at 858 ℃. With decreasing $P(O_2)$, the σ_{total} decreased in the high $P(O_2)$ range (region [A] and [B] in Figure 2a), was constant in the intermediate $P(O_2)$ range (region [C] in Figure 2a) and increased in the low $P(O_2)$ range (region [D] in Figure 2a). The slope of $\log(\sigma_{total})$ versus $\log(P(O_2))$ of $NdBaInO_4$ in the $P(O_2)$ range from 5.9×10^{-4} to 2.0×10^{-1} atm is 0.215(2) and of $Nd_{0.9}Sr_{0.1}BaInO_{3.95}$ in the $P(O_2)$ range from 5.7×10^{-3} to 2.0×10^{-1} atm is 0.216(6), which indicates that these materials show p-type conductivity in region [A], and mixed oxide-ion and hole conduction in region [B]. The constant conductivities independent of $P(O_2)$ in the region [C] indicate that both $NdBaInO_4$ and $Nd_{0.9}Sr_{0.1}BaInO_{3.95}$ materials show pure oxide-ion conduction.

Figure 2b shows Arrhenius plots of the total electrical conductivity σ_{total} (circles in Figure 2b) and oxide-ion conductivity σ_{ion} (triangles in Figure 2b) of NdBaInO$_4$ (black) and Nd$_{0.9}$Sr$_{0.1}$BaInO$_{3.95}$ (red). Over the entire temperature range, the total electrical conductivity σ_{total} and oxide-ion conductivity σ_{ion} of Nd$_{0.9}$Sr$_{0.1}$BaInO$_{3.95}$ are higher than those of NdBaInO$_4$. For example, the σ_{total} and σ_{ion} of Nd$_{0.9}$Sr$_{0.1}$BaInO$_{3.95}$ at 858 °C were 7.3×10^{-3} S cm^{-1} and 7.7×10^{-4} S cm^{-1}, respectively, are higher than those of NdBaInO$_4$ 1.0×10^{-3} S cm^{-1} and 3.6×10^{-5} S cm^{-1}, respectively. The hole conductivities of Nd$_{0.9}$Sr$_{0.1}$BaInO$_{3.95}$ and NdBaInO$_4$ were calculated as 6.5×10^{-3} and 9.6×10^{-4} S cm^{-1}, respectively, at 858 °C. The activation energies of total, oxide-ion, and hole conductivities of Nd$_{0.9}$Sr$_{0.1}$BaInO$_{3.95}$ were 0.685(7), 0.795(10), and 0.673 eV, which are lower than those of NdBaInO$_4$ (0.952(13), 0.91(4), and 0.953 eV). Therefore, 10 mol% Sr doping into NdBaInO$_4$ improves the oxide-ion conductivity and lowers its activation energy.

To investigate the structural changes in NdBaInO$_4$ by 10 mol% Sr doping, Rietveld analysis was conducted for Nd$_{0.9}$Sr$_{0.1}$BaInO$_{3.95}$ based on the synchrotron XRPD and NPD data using RIETAN-FP[12] and Z-Code.[13] Nd$_{0.9}$Sr$_{0.1}$BaInO$_{3.95}$ is isostructural with NdBaInO$_4$ (space group $P2_1/c$) and has seven independent sites at the general position, Nd, Ba, In, O1, O2, O3, and O4 (Table 2).8 The site preference of Sr was investigated in the preliminary analysis that gave the best reliable factors, R_{wp} and R_B, in the case that Sr exists at Nd site (Table S2 in Supplementary Information (SI)). Here, R_{wp} is a weighted reliability factor of profile intensity and R_B is a reliability factor based on integrated intensities. Therefore, the occupancy factors were fixed to g(Nd; Nd) = 0.9 and g(Sr; Nd) = 0.1 in the final refinement. Here, $g(Y; X)$ represents the occupancy factor of atom Y at the X site. The refinement of the occupancy factors of the oxygen atoms using common values
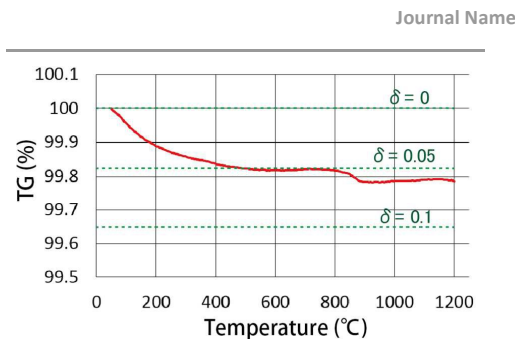
Figure 3. TGA curve of Nd$_{0.9}$Sr$_{0.1}$BaInO$_{3.95}$ measured in Ar. This figure shows the second cycle (first and third cycles are shown in SI). The green dash lines indicate the δ of Nd$_{0.9}$Sr$_{0.1}$BaInO$_{3.95-\delta}$. The weight loss from 50 to 800 °C was 0.18 wt%, which corresponds to the increase in oxygen vacancy content $\delta = +0.05$.

for all oxygen atoms yields 0.9842(10), which clearly indicates the existence of oxygen vacancies. The value agrees with the expected value of 0.9875 calculated from the charge balance. In the final refinement, the occupancy factors of oxygen atoms were fixed to 0.9875. The TGA of Nd$_{0.9}$Sr$_{0.1}$BaInO$_{3.95}$ showed 0.18% weight loss between 50 and 800 °C, which corresponds to $\delta = 0.05$ of Nd$_{0.9}$Sr$_{0.1}$BaInO$_{3.95-\delta}$ (Figure 3). Here, $(0.05+\delta)$ is the amount of oxygen vacancies. Thus, the occupancy factors of oxygen atoms were fixed to 0.975 for the high-temperature (800 °C) data. The final Rietveld patterns are shown in Figures 4a and 4b. The final refined atomic coordinates are shown in Table 1 for the TOF neutrons data and Table S1 in SI for the synchrotron X-ray and the angle dispersive type neutron data.

Comparing the unit-cell parameters between 24 °C and 800 °C, the a-, b- and c-axes increased and the β-angle decreased with increasing temperature. The average thermal expansion coefficients between 24 °C and 800 °C were found to be $\alpha_a = 1.23(4) \times 10^{-5}$ K^{-1}, $\alpha_b = 1.07(3) \times 10^{-5}$ K^{-1}, $\alpha_c = 0.72(4) \times 10^{-5}$
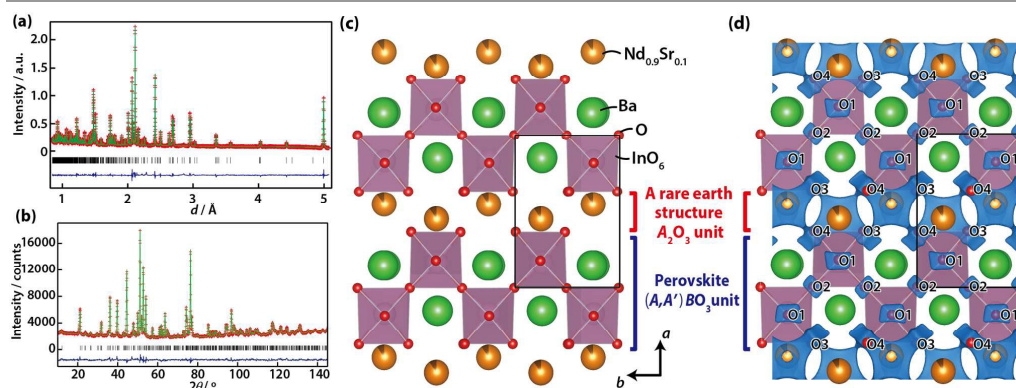
Figure 4. Rietveld patterns for NPD data of Nd$_{0.9}$Sr$_{0.1}$BaInO$_{3.95}$ taken at (a) 24 °C (iMATERIA) and (b) 800 °C (HRPD), showing the experimental (red + marks), calculated (green solid line) and difference (blue lower line) plots. Black tick marks indicate calculated Bragg peak positions. (c) Refined crystal structure of Nd$_{0.9}$Sr$_{0.1}$BaInO$_{3.95}$ at 24 °C viewed along the c-axis. The solid lines represent the unit cell. (d) Bond valence-based energy (BVE) landscape for an oxide ion with isovalue at 1.6 eV in Nd$_{0.9}$Sr$_{0.1}$BaInO$_{3.95}$ at 800 °C. Here, A and A' are relatively larger cations ((Nd,Sr) and Ba in this case) and B is a smaller cation (In in this case).

Journal Name

K^{-1}, $\alpha_\beta = -3.73(17) \times 10^{-5}$ K^{-1}, and $\bar{\alpha} = 1.06(2) \times 10^{-5}$ K^{-1} (the definition of these coefficients are described in section D of SI). These average thermal expansion coefficients of $Nd_{0.9}Sr_{0.1}BaInO_{3.95}$ are similar to those of $NdBaInO_4$ between 20 °C and 1000 °C ($\alpha_a = 1.42(2) \times 10^{-5}$ K^{-1}, $\alpha_b = 1.176(14) \times 10^{-5}$ K^{-1}, $\alpha_c = 0.77(3) \times 10^{-5}$ K^{-1}, $\alpha_\beta = -3.81(4) \times 10^{-5}$ K^{-1}, and $\bar{\alpha} = 1.176(15) \times 10^{-5}$ K^{-1}). There was an anisotropy observed in the thermal expansion. The average thermal expansion coefficients are similar for the a- and b-axes, whereas that of the c-axis is lower than the others. The average linear thermal expansion coefficients $\bar{\alpha}$ of $Nd_{0.9}Sr_{0.1}BaInO_{3.95}$ ($1.06(2) \times 10^{-5}$ K^{-1}) and $NdBaInO_4$ ($1.176(15) \times 10^{-5}$ K^{-1}) are close to that of yttrium stabilized zirconia (YSZ), which is favourable for using this material as a cathode in SOFC applications. The average thermal expansion coefficients of 3 and 8 mol% Y_2O_3-ZrO_2 between 20 and 1000 °C were reported as 1.08×10^{-5} and 1.05×10^{-5} K^{-1}, respectively.[14]

The crystal structure of $Nd_{0.9}Sr_{0.1}BaInO_{3.95}$ at 24 °C comprises the A rare earth structure A_2O_3 (($Nd,Sr)_2O_3$) and the perovskite $(A,A')BO_3$ (($Nd,Sr)_{2/8}Ba_{6/8}InO_3$) units (Figure 4c) which belongs to the same structural family as $NdBaInO_4$.[7] Here, A and A' are relatively larger cations and B is a smaller cation. The unit-cell volume at 24 °C of $Nd_{0.9}Sr_{0.1}BaInO_{3.95}$ ($443.184(2)$ $Å^3$) is slightly larger than that of $NdBaInO_4$ ($441.8905(3)$ $Å^3$). The larger volume is ascribed to the larger ionic radius[15] of Sr^{2+} (1.21 Å for coordination number (CN) of 7) than that of Nd^{3+} (1.046 Å for CN = 7). The calculated bond valence sums (BVSs)[16] from the bond lengths are 1.77 for Ba, 2.85 for ($Nd_{0.9}Sr_{0.1}$) and 2.99 for In sites in $Nd_{0.9}Sr_{0.1}BaInO_{3.95}$. These values are consistent with their formal charges 2, 2.9, and 3, respectively, which indicates the validity of the refined crystal structure of $Nd_{0.9}Sr_{0.1}BaInO_{3.95}$.

As described above, $Nd_{0.9}Sr_{0.1}BaInO_{3.95}$ contains oxygen vacancies, while there are no significant oxygen vacancies within the 3σ of refined occupancy in $NdBaInO_4$ at room temperature, where σ is the estimated standard deviation.[7] Considering that $Nd_{0.9}Sr_{0.1}BaInO_{3.95}$ has a much higher oxide-ion conductivity than $NdBaInO_4$, the dominant carrier for the oxide-ion conduction in $Nd_{0.9}Sr_{0.1}BaInO_{3.95}$ is the oxygen vacancy. The activation energy of the oxide-ion conduction is a little lower for $Nd_{0.9}Sr_{0.1}BaInO_{3.95}$ ($0.795(10)$ eV) than that for $NdBaInO_4$ ($0.91(4)$ eV). The lower activation energy of $Nd_{0.9}Sr_{0.1}BaInO_{3.95}$ is attributable to the larger bottleneck size for the oxide-ion diffusion path in $Nd_{0.9}Sr_{0.1}BaInO_{3.95}$ compared with $NdBaInO_4$. TGA of $NdBaInO_4$, and $Nd_{0.9}Sr_{0.1}BaInO_{3.95}$ showed little weight loss (around 0.02%) above 600 °C. Therefore, the effect of the carrier concentrations on the activation energy is thought to be negligible.

Diffusion pathways of oxide ions in the crystal structure of $Nd_{0.9}Sr_{0.1}BaInO_{3.95}$ and $NdBaInO_4$ were investigated by the bond valence based energy (BVE)[17] using the program 3DBVSMAPPER[18] based on the crystal structure at 800 °C. The blue surfaces in Figure 4d represent the isosurfaces where the BVE for an oxide ion is +1.6 eV. In this landscape, the most stable position (at O4) was set to 0 eV. BVE isosurfaces around O1 and O2 sites are localized, while those around O3 and O4 sites spread into the A rare earth structure A_2O_3 (($Nd,Sr)_2O_3$)

unit and are connected with each other along both the b- and c-axes. The lowest energy path for oxide-ion conduction in $Nd_{0.9}Sr_{0.1}BaInO_{3.95}$ was found to be along the b-axis with an energy barrier of 1.42 eV. The energy barriers of the path along the a- and c-axes were calculated to be 2.72 and 1.47 eV for $Nd_{0.9}Sr_{0.1}BaInO_{3.95}$. The paths along the b- and c-axes have similar energy barriers and the path along the a-axis has significantly higher energy barrier than the others. Thus, the oxide-ion conduction in $Nd_{0.9}Sr_{0.1}BaInO_{3.95}$ would be two dimensional.

BVE barriers of $Nd_{0.9}Sr_{0.1}BaInO_{3.95}$ have lower values than those of $NdBaInO_4$ along the oxide-ion diffusion paths. The energy barriers along the a-, b- and c-axes calculated based on the crystal structures at 24 °C are 1.47, 2.88, and 1.69 eV for $Nd_{0.9}Sr_{0.1}BaInO_{3.95}$ and 1.72, 3.95, and 2.01 for $NdBaInO_4$. These results are consistent with the experimental data that showed that $Nd_{0.9}Sr_{0.1}BaInO_{3.95}$ has lower activation energy of oxide-ion diffusion than $NdBaInO_4$. The highest BVE point along the possible oxide-ion diffusion path is surrounded by two (Nd or (Nd,Sr)) and one Ba cations, which forms a cation triangle bottleneck. The areas of the triangles were calculated to be $6.889(5)$ $Å^2$ for $NdBaInO_4$ and $6.911(3)$ $Å^2$ for $Nd_{0.9}Sr_{0.1}BaInO_{3.95}$. Thus, the substitution of Nd with Sr increases this bottleneck area, and hence, lowers the activation energy of oxide-ion conduction.

CONCLUSIONS

The oxide-ion conductivity has been increased and the activation energy of oxide-ion conduction has been lowered by the substitution of Nd with Sr cations in $NdBaInO_4$. $Nd_{0.9}Sr_{0.1}BaInO_{3.95}$ showed highest electrical conductivity among $Nd_{1-x}Sr_xBaInO_{4-x/2}$ ($x = 0.0, 0.1, 0.2$ and 0.3). The oxide-ion conductivity σ_{ion} of $Nd_{0.9}Sr_{0.1}BaInO_{3.95}$ was 7.7×10^{-4} S cm^{-1} at 858 °C, which is higher than that of $NdBaInO_4$ ($\sigma_{ion} = 3.6 \times 10^{-5}$ S cm^{-1} at 858 °C). The crystal structure of $Nd_{0.9}Sr_{0.1}BaInO_{3.95}$ has been analysed, and we have confirmed that Sr exists at Nd site. $Nd_{0.9}Sr_{0.1}BaInO_{3.95}$ contains oxygen vacancies, which were not observed for $NdBaInO_4$ at room temperature. Thus, the increase of the oxide-ion conductivity is mainly attributed to the increase of the carrier concentration. BVE calculations indicated two-dimensional oxide-ion diffusion in the A_2O_3 (($Nd,Sr)_2O_3$) unit on the bc-plane and a decrease of the energy barrier by the substitution of Nd with Sr cations.

ACKNOWLEDGMENTS

Notes and references

[a] Department of Chemistry and Materials Science, Graduate School of Science and Engineering, Tokyo Institute of Technology, 2-12-1-W4-17, O-okayama, Meguro-ku, Tokyo 152-8551, Japan
[b] Department of Chemistry, Graduate School of Science and Engineering, Tokyo Institute of Technology, 2-12-1-W4-17, O-okayama, Meguro-ku, Tokyo 152-8551, Japan
[c] Neutron Science Division, Research Reactor Utilization Department, Korea Atomic Energy Research Institute, 1045 Daedeok-daero, Yuseong-gu, Daejeon, 305-353, Korea

Electronic Supplementary Information (ESI) available: A document containing the crystallographic data of $Nd_{0.9}Sr_{0.1}BaInO_{3.95}$, additional experimental information, and a crystallographic information file (CIF) of $Nd_{0.9}Sr_{0.1}BaInO_{3.95}$.

1. (a) J. B. Goodenough, *Nature*, 2000, **404**, 821; (b) J. B. Goodenough, *Annu. Rev. Mater. Res.*, 2003, **33**, 91; (c) V. Thangadurai, W. Weppner, *Ionics*, 2006, **12**, 81; (d) D. J. L. Brett, A. Atkinson, N. P. Brandon, S. J. Skinner, *Chem. Soc. Rev.*, 2008, **37**, 1568; (e) L. Malavasi, C. A. J. Fisher, M. S. Islam, *Chem. Soc. Rev.*, 2010, **39**, 4370; (f) S. Y. Istomin, E. V. Antipov, *Russian Chem. Rev.*, 2013, **82**, 686; (g) A. B. Muñoz-García, A. M. Ritzmann, M. Pavone, J. A. Keith, E. A. Carter, *Acc. Chem. Res.*, 2014, **47**, 3340.

2. (a) J. C. Boivin, G. Mairesse, *Chem. Mater.*, 1998, **10**, 2870; (b) J. A. Kilner, M. Burriel, *Annu. Rev. Mater. Res.*, 2014, **44**, 365.

3. (a) M. Mogensen, D. Lybye, N. Bonanos, P. V. Hendriksen, F. W. Poulsen, *Solid State Ionics*, 2004, **174**, 279; (b) M. Yashima, *Solid State Ionics*, 2008, **179**, 797.

4. (a) A. S. Bhalla, R. Guo, R. Roy, *Mat. Res. Innovat.*, 2000, **4**, 3; (b) R. E. Schaak,; T. E. Mallouk, *Chem. Mater.*, 2002, **14**, 1455; (c) S. Stølen, E. Bakken, C. E. Mohn, *Phys. Chem. Chem. Phys.*, 2006, **8**, 428; (d) M. Yashima, *J. Ceram. Soc. Jpn.*, 2009, **117**, 1055.

5. (a) V. V. Kharton, A. P. Viskup, E. N. Naumovkh, F. M. B. Marques, *J. Mater. Chem.*, 1999, **9**, 2623; (b) S. Miyoshi, T. Furuno, O. Sangoanruang, H. Matsumoto, T. Ishihara, *J. Electrochem. Soc.*, 2007, **154**, B57; (c) T. Ishihara, K. Nakashima, S. Okada, M. Enoki, H. Matsumoto, *Solid State Ionics*, 2008, **179**, 1367; (d) M. Yashima, M. Enoki, T. Wakita, R. Ali, Y. Matsushuta, F. Izumi, T. Ishihara, *J. Am. Chem. Soc.*, 2008, **130**, 2762; (e) M. Yashima, N. Sirikanda and T. Ishihara, *J. Am. Chem. Soc.*, 2010, **132**, 2379; (f) M. Yashima, H. Yamada, S. Nuansaeng and T. Ishihara, *Chem.*

Mater., 2012 **24**, 4100; (g) K. Kawamura, M. Yashima, K. Fujii, K. Omoto, K. Hibino, S. Yamada, J.R. Hester, M. Avdeev, P. Miao, S. Torii, T. Kamiyama, *Inorg. Chem.*, 2015, **28**, in press, DOI: 10.1021/acs.inorgchem.5b00102.

6. X. Kuang, M. A. Green, H. Niu, P. Zajdel, C. Dicknson, J. B. Claridge, L. Jantsky, M. J. Rosseinsky, *Nat. Mater.*, 2008, **7**, 498.

7. (a) S. Nakayama, M. Sakamoto, *J. Eur. Ceram. Soc.*, 1998, **18**,1413; (b) M. Higuchi, Y. Masubuchi, S. Nakayama, S. Kikkawa, K. Kodaira, *Solid State Ionics*, 2004, **174**, 73; (c) R. Ali. M. Yashima, Y. Matsushita, H. Yoshioka, K. Ohoyama, F. Izumi, *Chem. Mater.*, 2008, **20**, 5203.

8. K. Fujii, Y. Esaki, K. Omoto, M. Yashima, A. Hoshikawa, T. Ishigaki, J. R. Hester, *Chem. Mater.*, 2014, **26**, 2488.

9. http://www.spring8.or.jp/wkg/BL19B2/instrument/lang-en/INS-0000000300/instrument_summary_view

10. T. Ishigaki, A. Hoshikawa, M. Yonemura, T. Morishima, T. Kamiyama, R. Oishi, T. Sakuma, Y. Tomota, M. Arai, M. Hayashi, K. Ebata, Y. Takano, H. Asano, Y. Takano, T. Kasao, *Nucl. Instrum. Methods Phys. Res., Sect. A*, 2009, **600**, 189.

11. https://hanaro.kaeri.re.kr:444/NB/sub02/sub02.do

12. F. Izumi, K. Momma, *Solid State Phenom.*, 2007, **130**, 15.

13. (a) R. Oishi, M. Yonemura, Y. Nishimaki, S. Torii, A. Hoshikawa, T. Ishigaki, T. Morishima, K. Mori, T. Kamiyama, *Nucl. Instrum. Methods Phys. Res., Sect. A*, 2009, **600**, 94; (b) R. Oishi-Tomiyasu, M. Yonemura, T. Morishima, A. Hoshikawa, S. Torii, T. Ishigaki, T. Kamiyama, *J. Appl. Cryst.*, 2012, **45**, 299.

14. I. Yasuda, M. Hishinuma, *Electrochem.*, 2000, **68**, 526.

15. R. D. Shannon, *Acta Crystallogr.*, 1976, **A32**, 751.

16. R. E. Brese, M. O'Keeffe, *Acta Crystallogr.*, 1991, **47**, 192.

17. (a) S. Adams, *Solid State Ionics*, 2000, **136**, 1351. (b) S. Adams, *Struct. Bond.*, 2014, **158**, 91; (c) M. Avdeev, M. Sale, S. Adams, R. P. Rao, *Solid State Ionics*, 2011, **225**, 43.

18. (a) M. Sale, M. Avdeev, *J. Appl. Crystallogr.*, 2012, **45**, 1054; (b) M. Yashima, N. Kubo, K. Omoto, H. Fujimori, K. Fujii, K. Ohoyama, *J. Phys. Chem. C*, 2014, **118**, 5180; (c) M. Yashima, T. Sekikawa, D. Sato, H. Nakano, K. Omoto, *Cryst. Growth Des.*, 2013, **13**, 829; (d) M. Yashima, "Invited Review: Some recent developments in the atomic-scale characterization of structural and transport properties of ceria-based catalysts and ionic conductors", *Catal. Today*, 2015, in press.